International Forum on Aeroelasticity and Structural Dynamics
IFASD 2024
17-21 June 2024, The Hague, The Netherlands

GUST LOAD ALLEVIATION WIND TUNNEL TESTS OF A FOLDING WING TIP CONFIGURATION

L. Marchetti[1], S. Ricci[1], L. Riccobene[1], D. Grassi[1], P. Mantegazza[1], S. Adden[2], H. Gu[3], and J.E. Cooper[3]

[1] Politecnico di Milano, Piazza Leonardo da Vinci 32, 20133, Milano, Italy
[2] IBK Technologies GmbH & Co, KG, 21129 Hamburg, Germany
[3] University of Bristol, Dept of Aerospace Engineering, Bristol, BS8 1TR, United Kingdom

Keywords: Aeroelasticity, wind tunnel, gust alleviation, high aspect ratio, experimental

Abstract: Increasing the aspect ratio is one way to improve aircraft aerodynamic efficiency. This reduces the induced drag term but, at the same time, produces an increment of the wing loads, hence an increase of the structural weight. This paper reports the results obtained during a dedicated experimental campaign inside the large wind tunnel at Politecnico di Milano exploring the gust load alleviation capability of a folding wing tip device. This activity has been done under the umbrella of CS2-U-HARWARD project. The high aspect ratio wing equipped with this device was mounted on a half aircraft lying on its side. The model could freely rotate around its pitching axis and a sledge allowed the entire model to plunge. An electromagnetic actuator allowed the application of a dummy weight force to the aircraft counteracting the lifting force, hence permitting the trim of the aircraft. The gusts were produced by deflecting six vanes in front of the model, with different gust lengths produced to excite different frequencies of the wing. A pneumatic actuator was used to keep the wing tip in its standard configuration and release the mechanism allowing it to fold at will. Several delays between the triggering of the gust and the release of the hinge mechanism were tested, to assess the coupling between the dynamics induced by the gust and the one induced by the release of the mechanism. Three strain gauge bridges were installed on the spar of the wing to measure the bending moment at three different sections corresponding to the root, the engine and as near as possible to the hinge. In addition, a camera tracking system composed of six infrared cameras allowed the reconstruction of the 3D motion of the wing hit by the gust and the complex dynamics of the folding wingtip. The measured wing root bending moment shows that the amount of load alleviation depends on the time when the gust hits the folding wing tip. The wing tip needs to be free to float when the gust hits it for the alleviation to be effective, but the transient of the unlocking of the hinge seems to be beneficial to the goal.

1 INTRODUCTION

The impacts of climate change are clear and evident in our everyday life and explain the worldwide effort in trying to reduce the most relevant cause of these changes, in particular, the use of carbon-based fuels for all energy-related societal activities, including transport and aviation. This need has been identified by ICAO, FLIGHTPATH2050 and Clean Sky 2 initiatives in Europe and also NASA, with challenging goals set for reductions in CO2, NOX and noise by the year

2050 [1] [2] [3]. The aviation world is well aware of these climate targets and has for many years undertaken activities to move towards electric, sustainable aviation fuel and hydrogen-powered aircraft; however, it will be impossible to achieve net zero emissions by 2050, and therefore, other measures will need to be implemented.

The Aerospace Technology Institute (ATI) "Destination Zero" strategy [4] determined the amount of carbon reduction that needs to be achieved by: reducing tailpipe emissions (more efficient aircraft designs and engines), reducing life cycle fuel use (better Air and Ground traffic management) and eliminating residual emissions through the use of SAF or hydrogen. The Air Transport Action Group (ATAG) [5] expressed similar findings for three different scenarios for achieving net zero – i. pushing technology and operations, ii. Aggressive sustainable fuel deployment, and iii. an aspirational and aggressive technology perspective. These scenarios defined reductions in fuel burn of 22%, 12%, and 34%, respectively, with the latter scenario being particularly challenging.

Consideration of the development of more fuel-efficient and environmentally friendly aircraft designs required to meet these targets has been the focus of the U-HARWARD project. However, the rate of improvement in the performance of conventional aircraft configurations (via improved aerodynamics, lightweight structures, and better engines) is not fast enough to achieve net zero aviation by 2050. As a consequence, the need to explore the benefits of novel aircraft architectures to provide a step-change in fuel efficiency is evident.

The move towards higher aspect ratio wing designs to reduce induced drag will require the use of folding wingtips to meet airport gate and taxi limits, as seen on the B777-X. The consequent requirement for a hinge has led to the feasibility of the use of floating folding wingtips in-flight [6] to reduce the effect of gust and turbulence loads whilst still improving the aerodynamic performance. Many numerical studies have been validated by several wind tunnel experiments to demonstrate the gust load alleviation [7, 8], nonlinear geometric effects [9, 10], and roll performance [11]. Further experimental validation of the concept involved the AlbatrossONE flight test model [12] (the first flight tests of the SAH concept in-flight), which implemented the folding wingtips in a way, known as the Semi-Aeroelastic Hinge (SAH), such that the wing-tip release is delayed until the gust field is encountered. Such an implementation aims to optimize both aerodynamic and gust alleviation performance. Numerical studies on gust responses [13, 14, 15] and some initial wind tunnel tests at TU Delft [16] indicate that the gust load alleviation performance of the SAH depends upon when the wingtip is released where it is found that there is a 'sweet spot' in the release time to allow for optimum load alleviation, resulting in the minimum wing loads.

In this work, experimental wind tunnel tests using a large (2m) half-aircraft model are reported investigating the performance of a flexible wing incorporating a folding wingtip when subjected to a controllable gust field. This is the first time that the Semi Aeroelastic Hinge (SAH) approach has been implemented on such a large wind tunnel model with heave and pitch degrees of freedom as well as a flexible wing. The wind tunnel model was obtained from a scaled A321-like aircraft using an iso-frequency approach. The gust load alleviation performance of the SAH was then assessed for various gust lengths, wind speeds, trim angles, and folding wing tip release times relative to the approaching gust.

2 THE U-HARWARD PROJECT

The path towards a completely carbon neutral air transport will certainly take many years and will require several intermediate steps. Although the recent announcement by Airbus of the zero-emission program, with the promise of flying the first fully hydrogen-powered aircraft by 2035, it is clear that there will be a transition through more traditional architectures but with a higher level of efficiency, certainly possible even with the technologies already available at the moment. Targeting this intermediate goal, the CS2-U-HARWARD project started in May 2020 in response to the call JTI-CS2-2019-CFP10-THT-07: Ultra-High Aspect ratio wings, aiming at the use of innovative aerodynamic and aeroelastic designs in a multi-fidelity multi-disciplinary optimal design approach to facilitate the development of Ultra-High aspect ratio wings for medium and large transport aircraft.

The consortium of U-HARWARD is composed of six partners: Politecnico di Milano, the coordinator, IBK-Innovation GmbH & Co. KG, University of Bristol, Office National d'Etudes et de Recherches Aérospatiales, Institut Supérieur de l'Aéronautique et de l'Espace and Siemens Industry Software SAS. The main idea of U-HARWARD project is to combine the modern design and manufacturing technologies to extend the actual span limit of conventional configurations, together with a deep investigation on a new, promising configuration, i.e. The Strut-Braced Wing (SBW) and finally with the feasibility studies of a new disrupting technology based on the active folding wingtip concept. To this aim, the design activities range from the conceptual up to the high fidelity level and are managed by three teams focusing on three different concepts. Team 1, composed by Politecnico di Milano and IBK, is focused on traditional cantilever wing configurations with extended aspect ratio. Team 2, composed of ONERA and ISAE, is focused on the Strut-Braced Wing configuration. Finally, Team 3 represented by the University of Bristol and Siemens, is mainly focused on folding wing tip configuration [17].

3 THE REFERENCE AIRCRAFT

U-HARWARD design activities have been organized in a parallel way: 3 teams evaluated separately the 3 design options mentioned above, and results will be gathered and compared at the end of the OAD studies, to derive common conclusions and requirements for next phase of the project involving high fidelity analysis and optimization and experimental validation. Therefore, there was a need for a common reference among the teams to calibrate design tools and enable direct comparison of results. This reference aircraft is also used to position the results of the project and communicate on them. Defining a reference aircraft relies on 2 separate aspects: the mission to be completed by the aircraft, which often relies on some market segments in the aeronautics industry: regional, short-medium range, long range; the technology level and detailed features to be implemented on this reference aircraft: copy-paste of an existing one, redesign of a new aircraft, targeted EIS and associated technology levels. As no market segment is explicitly specified in the U-HARWARD targets, a broad analysis has been conducted to choose the most relevant mission definition, both from the benefits we can expect for a future commercialized aircraft, and from the more general lessons we could derive with the studies conducted in U-HARWARD.

The A320 family is well known by the research community, especially through the numerical model CeRAS CSR-01, and serves as a basis for comparison for a lot of CS2 studies. However, the typical mission of such an aircraft has a very short cruise segment and the benefits of a UHARW might not be maximal. Therefore, it was decided to go for the extended SMR segment, which is the one of the A321, to combine the demonstration of high benefits in this “middle of the

market" segment, and the possible transposition to smaller (eg. SMR and even regional) or bigger aircraft. Therefore, the choice was oriented towards the A321neo aircraft.

This reference aircraft has been re-designed by the teams by first taking benefit of the existing database of CeRAS CSR-01, then stretching the results to the A321 neo results with modified fuselage and engine, upon the specific TLAR. Finally, 2035 technology options have been introduced at the end of the project for comparison with other CS2 studies.

Figure 1: The model inside the wind tunnel

4 THE WIND TUNNEL MODEL

The wind tunnel model is a half aircraft mounted on a pivot on a sled, allowing the pitch and heave motion. Everything but the wing comes from previous projects (WTT3 tests in the CS2-AIRGREEN2 project [18] [19], developed from the CS1-GLAMOUR project [20]). The half-span is 2.17 meters, the total length is 4.8 meters. The folding span is one fourth of the total length of the wing.

4.1 Wind Tunnel model scaling

Given the already existent fuselage, a geometric scaling factor of 1:10 was chosen so that the wing could fit the joint with the fuselage. While traditionally a constant Froude number approach is adopted, in this case an iso-frequency approach was preferred. This choice was made because all previous gust response tests based on the same platform had a model scaled this way and this gave us confidence on the capability of the gust generator to reproduce the required gusts.

Scaling factors for the iso-frequency approach are summed up in the following table, where λ is equal to 1/10, in this case.

Table 1: Scaling factor used for the wind tunnel model

Parameter	Units	Scale factor ($\boldsymbol{\lambda}$)
Geometric similarity		
Length	L	λ
Area	L^2	λ^2
Volume	L^3	λ^3
Rotation	-	1
Kinematic similarity		
Time	T	1
Velocity	LT^{-1}	λ

Acceleration	LT^{-2}	λ
Dynamic similarity		
Mass	M	λ^3
Force	MLT^(-2)	λ^4
Moment	ML^3 T^(-2)	λ^6
Pressure/Stress	ML^(-1) T^(-2)	λ^2
Frequency	T^(-1)	1
Density	ML^(-3)	1

4.2 The wing

The external shape of the reference wing is reproduced with aerodynamic sectors attached to a single spar in just one-point spanwise so that the only contribution to the overall stiffness is given by the spar. This design philosophy is adopted to decouple aerodynamics and stiffness and simplify both the design phase and the finetuning after the manufacturing.

Six aerodynamic sectors are used to discretize the aerodynamic shape, plus a cover for the connection with the fuselage.

4.2.1 The spar

The wing is divided into three main parts, from a structural point of view. The wingtip requires a too low stiffness to be reproduced correctly and, since it is not extremely important for the dynamics of the gust, no correct scaling is applied. The wingtip has no main spar and is a solid piece of 3D printed Windform XT2. The inboard part of the wing is divided into two parts: in the inboard region the size of the cross-section is large enough to have a complex shape composed by a solid rectangular with flanges and all three stiffnesses EIx, EIy and GJ are reproduced correctly, while in the outboard region the thickness of the flanges would be too low to be manufactured, and the cross-sections becomes a simple rectangle reproducing out-of-plane bending stiffness and torsional stiffness. The material used is a milled glass fiber which allows complex shapes and a continuous variation of cross-cross section to better follow the reference stiffness distribution.

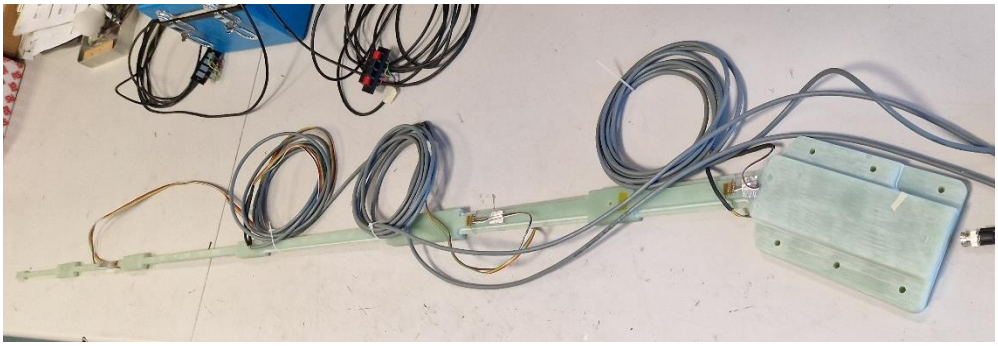

Figure 2: the spar with the strain gauges installed

4.2.2 The engine

To account for the real engine weight a scaled engine mass model was designed. The center of gravity of the scaled engine mass assembly was designed to meet the exact scaled center of gravity location with respect to the real engine.

To represent the engines moment of inertia (Iyy and Izz) correctly on the wind tunnel model, a dumbbell-like mass assembly with lead weights is mounted to a steel pylon. A steel bracket is used

to tightly connect this with the wing spar. A bolt in the center of the bracket prevents movement along the wing spar axis.

4.2.3 The aerodynamic sectors

The wing model assembly consists of six separate 3D printed aerodynamic sectors. All but the wing tip one are fixed to the wing spar. The wing tip is connected to the release mechanism, which is fastened to the end of the wing spar.

Between all wing sectors a small gap is left to prevent contact with each other during testing, allowing the intended aeroelastic deflection of the wing.

Figure 3: a 3D printed aerodynamic sector

4.2.4 The wing tip release mechanism

The main function of the mechanism is executed by a pneumatic piston, that pushes on a bolt with a conical head into a respective conical pocket on the hinge part of the wing tip.

Figure 5: the locking mechanism

By pushing the bolt into the pocket on the wing tip hinge part, the wing tip is locked in its original straight position. On command this bolt can be retracted from the pocket to release the wing tip to be able to rotate freely around the hinge axis.

4.3 The rest of the aircraft

The rest of the aircraft comes from the previous tests in the CS2-AIRGREEN2 project, that is the last iteration of the original CS1-GLAMOUR project.

4.3.1 The weight augmentation system

The wind tunnel model, representing half of the reference aircraft, is connected to the floor with dedicated support able to guarantee a free-free motion in pitch and heave. This configuration appears challenging from the model trim point of view, due to the presence of the *1g* loads. Indeed, since the wing is in a vertical position the weight does not offer any counterbalance of the lift force. The adopted strategy required the use of a dedicated device able to produce the necessary force able to balance the lift produced at different test speeds. The name of this device is Weight Augmentation System (WAS) that was conceived and manufactured during the EU project CS1-GLAMOUR. It is composed of a sliding mechanism that allows for the heave motion driven by an electrical servo-actuator controlled in force, as to be able to guarantee a constant force,

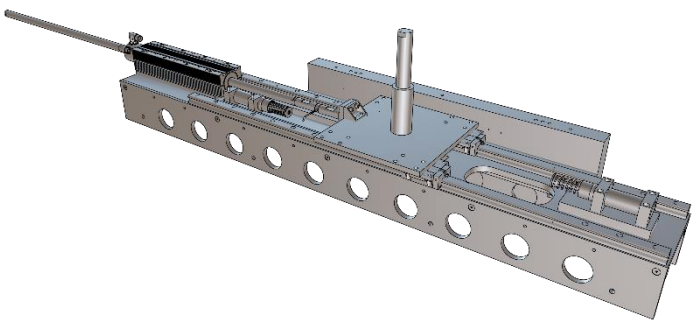

Figure 4: the Weight Augmentation System

corresponding to the *1g* trim loads. Thanks to this system, it is possible to trim the model for different flight conditions so to assess the validity of the gust alleviation strategies for a large portion of the flight envelope. The hardware constituting the WAS system is covered by the so-called dummy floor over which the wind tunnel model is sliding in pitch and heave motion.

4.3.2 The fuselage and the tail

The main structural component of the fuselage is a composite beam of hollow square cross-section spanning from nose to tail but split into two parts connected together at the central wing root region. The beam is manufactured in composite (carbon fibre) to obtain natural frequencies well above those of the wing, minimizing couplings and undesired excitation of the system. The two halves of the beam are bolted together to a connecting aluminium insert. The hollow square beam fits snugly within the composite beam and defined the bolting region for the wing support. From the perspective of fuselage skins, the outer surfaces are defined by three main components: a front fuselage section, a rear fuselage, and the fuselage nose. All of them are in composite, but their draping and thickness differ. The nose is made by a light glass fibre skin since it is used just to close the fuselage and not special loads are applied to it. The central and rear parts of the fuselage skins are made by carbon fabric reinforced by rohacell to increase the global stiffness to have the fuselage mode shapes at a well higher frequency than the ones of the wing. Ten carbon fibre and wooden ribs form the internal part of the fuselage covers. These reinforcement elements have the purpose of supporting the otherwise large external panel. In this way, the skin panels are partitioned into smaller ones, and hence increasing the buckling eigenvalues. The vertical tail sub-assembly stems from the rear end of the fuselage beam. An aluminum beam with a rectangular section introduces the desired cone angle and is attached employing a U-shaped bracket setting in the composite beam. Upwards shoot two spars and an enforcing plate component. Together these elements define the vertical tailplane, which is subsequently crowned by the trimming mechanism. Such a mechanism is composed of a machined plate and two brackets which form the axis for the rotation of the horizontal tail. An arm also extends aft to position the elevator actuator, allowing for the cohesive rotation of both lifting and control surfaces. A spar extends outwards to assemble the horizontal tail. The structural solution adopted for the horizontal tailplane is similar to the one adopted for other components, i.e. a sandwich structure made of carbon fibre skin and a Nomex core. Three hinges were embedded in the core, and all components were bolted to the skin. The hinges provide support for the elevator, which was built in the same way as the wing 3D printed sectors. The control and acquisition systems

Figure 6: the fuselage and the tailplanes

4.3.3 The installed instrumentation

The experimental instrumentation used during wind tunnel test was the following:

- 1 onboard PC-104 for acquisition and control of the model
- 18 uniaxial accelerometers
- 1 encoder for pitch angle
- 1 potentiometer for sled position
- 1 load cell for trim force
- 3 half bridges for bending load
- 3 full bridges for torsion load
- 1 PXI system for bridges acquisition
- 6 Miqus M3 infrared cameras, 100 Hz, for marker tracking
- 39 optical markers
- 1 PC for tracking system acquisition
- 1 PC for WAS (weight augmentation system) control

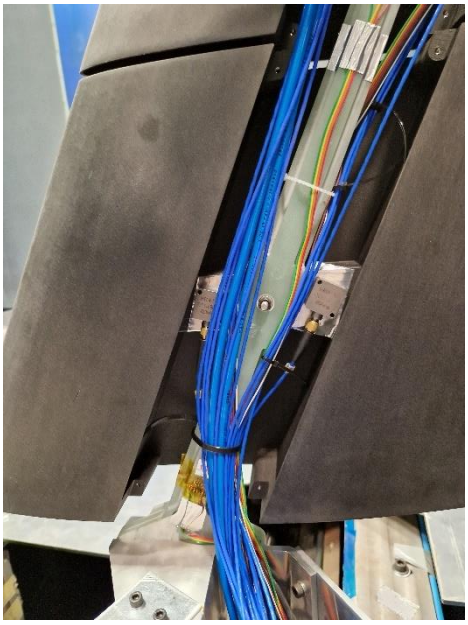

Figure 8: root section of the wing

Six cameras are mounted on a wall, framing the entire wing, its connection to the fuselage and part of the gust generator. To capture the motion of the model, four markers are placed on each aerodynamic sector (three is the minimum to recover the rigid body motion, the fourth one is for redundancy). The wing tip has two additional markers to better locate its tip and its root. Two markers are placed on the hinge, one on the leading edge and one on the trailing edge. Six markers are placed on the fuselage near the wing. The entire model is considered to be rigid, so just three markers would be necessary, but with six it's sure that at least three are always inside the frame, no matter the attitude of the aircraft. Four markers are placed on the floor of the test room to have a fixed reference for the model. A total of 18 uniaxial accelerometers are installed in the model. There are two for each aerodynamic sector of the wing, measuring the out-of-plane acceleration. This way it is possible to monitor out-of-plane bending and torsion of the wing. Two accelerometers are placed on the dummy engine, measuring the out-of-plane and in-plane directions. One accelerometer is placed on the sled to record the rigid body acceleration of the model. One accelerometer is placed inside the wing tip. Two accelerometers are placed on the horizontal tail, one at the root and one at the tip,

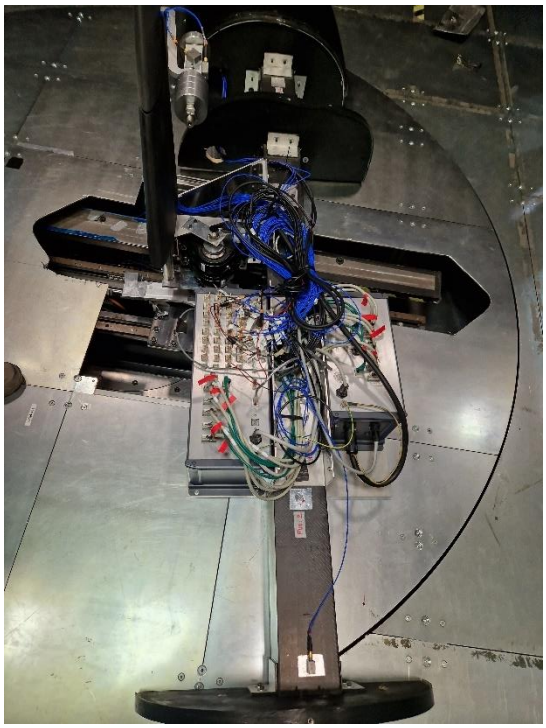

Figure 7: the onboard acquisition system

measuring in the out-of-plane direction. Two additional accelerometers are placed inside the fuselage, one near the nose and one near the tail. They measure along the same direction as the other accelerometers inside the model, so that the angular velocity and acceleration of the aircraft can be derived.
Extensometer bridges are installed on the main spar to measure the bending moment and the torque at three different spanwise locations. The most important section for this test is the root section, but two more are added, one just before the connection to the dummy engine and one as near as possible to the hinge.

A pneumatic actuator locks the hinge of the wing tip and is controlled by a solenoid valve placed under the test room.

4.3.4 The acquisition and control systems

Every acquisition and control system other than the onboard one, is placed under the test room.

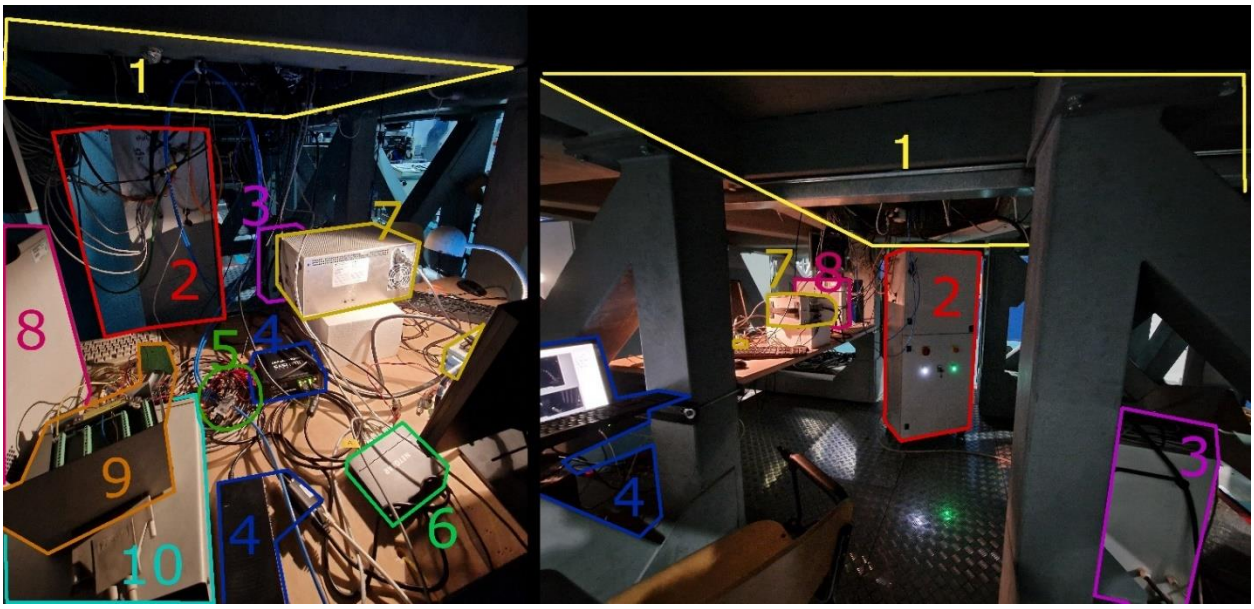

Figure 9: test setup under the test room

1. Floor of the test room
2. Power supply and drivers for the electromagnetic actuators (both sled and gust generator)
3. Power supply for the onboard pc and for the driver of the motor of the elevator
4. Camera tracking acquisition and synchronization units
5. Solenoid valve for the pneumatic actuator to unlock the hinge
6. LAN hub to control everything from the control room
7. Pxi system to acquire the bridges measurements
8. Pc to control the sled
9. Acquisition of the load cell and of the potentiometer
10. Power supply for the potentiometer, the load cell, and the solenoid valve

5 THE GROUND VIBRATION TEST

5.1 The test setup

The setup adopted was composed by 2 frontend Scadas 316, 21 uniaxial and 17 triaxial accelerometers, a Bruel&Kjaer Type 4809 shaker, and the entire test management was done using Software LMS-TestLab. All the GVT tests on the aeroelastic model were performed in the test chamber of the Large POLIMI's wind tunnel. The number and position of the installed accelerometers were chosen according to considerations concerning the need to obtain clear information about the modal shapes. The purpose was to correctly recover the in-plane and out-of-plane bending shapes of the wing and of the horizontal tail plane, as well as the torsional ones. Even if the fuselage and the vertical tail were supposed rigid, investigation of their real behaviour was performed. Seventeen measuring locations were identified on the wing, seven on the horizontal tail plane, six on the vertical tail plane, two on the engine and five on the fuselage.

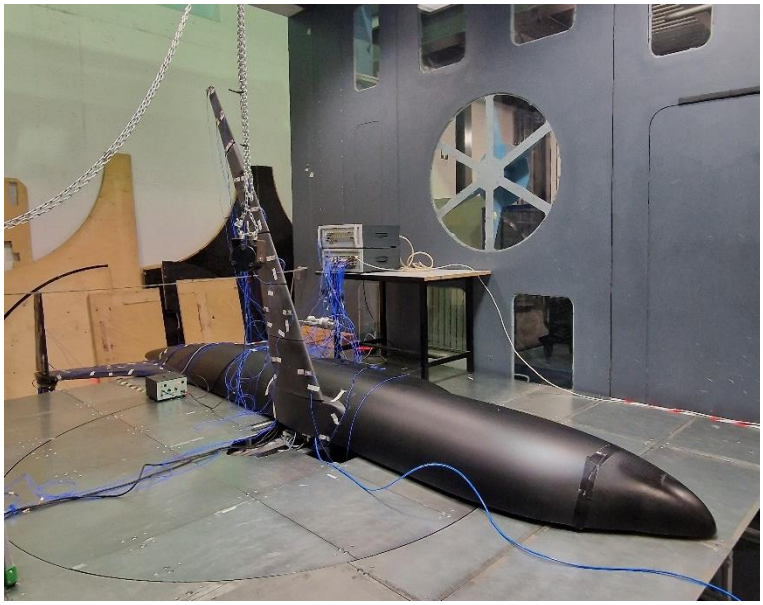

Figure 10: the GVT test setup

A shaker test was performed to acquire FRFs. A stepped-sine excitation in open-loop methodology was employed. The frequency range between 1 Hz and 20 Hz was investigated with a frequency resolution of 0.025 Hz along all the band. The FRFs were estimated by H_v method.

Finally, Modal identification was carried out with software LMS-TestLab Rev.17 using the algorithm Polymax^{TM}.

5.2 The GVT results

The GVT results, in terms of frequency, modal damping and shapes are summarized in the following table.

Table 2: GVT Results

Mode	Frequency Hz	Damping %	Generalized Mass
1	1.317	0.93	0.827
2	1.626	1.37	2.141
3	2.845	1.57	9.993
4	5.346	1.31	1.290
5	6.305	1.22	0.518
6	6.780	3.75	0.762

7	7.556	0.88	11.920
8	9.796	1.38	2.981
9	11.974	1.90	0.779
10	13.036	1.74	0.568
11	15.945	3.40	2.491
12	16.937	1.72	2.282
13	17.513	1.24	1.148
14	18.199	3.36	1.584

6 THE WIND TUNNEL AND THE GUST GENERATOR

6.1 The Wind Tunnel

The GVPM (Galleria del Vento Politecnico di Milano) is a medium-size low-speed wind tunnel highly dedicated to helicopter and airplane model testing. Due to this facility, POLIMI is a member of SATA since 2003. The wind tunnel can operate both in a closed test section and in an open jet configuration. The closed test section is 6 m long, 4 m wide and *3.84 m* high. The first *5 m* part of the closed test section is removable to allow for off-line test preparation (or, in case, to allow for open jet tests). Two interchangeable closed test sections (the ”yellow” and the ”blue” one) are available. A high flow ratio compressor supplies compressed air for the air-bearing movement systems that are used to move the closed test sections and the other heavy structures or machines. The flow quality is adequate for aeronautical testing (the turbulence level is less than 0.1%). The airflow is produced by 14 fans with a total power of 1.4 MW. By virtue of the heat exchanger, the wind tunnel testing is not affected by any significant temperature gradient so that test duration is not limited by wind tunnel overheating. The wind tunnel is controlled in velocity (from *3 m/s* up to *55 m/s*). The maximum velocity of *55 m/s* corresponds to a maximum Mach number of *0.16* and to Reynolds number per meter of about *3.8* million. As this usually produces a model Reynolds number lower than in the full-scale aircraft, transition strips can be positioned on the model surface. Adhesive tape transition strips are used at GVPM, sized according to NASA TN-3579.

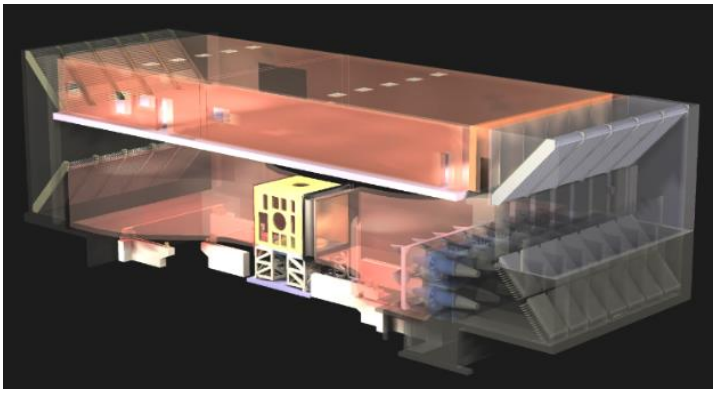

Figure 11: the GVPM wind tunnel

The velocity feedback for the control is obtained by dynamic pressure measurement together with the measurement of thermodynamic quantities necessary to compute the fluid density. The test condition parameters continuously monitored during the test are dynamic pressure, absolute pressure, absolute temperature, and relative humidity. Thus an accurate evaluation of the actual fluid density is possible allowing the flow velocity to be obtained from the dynamic pressure.

6.2 The gust generator

To perform the gust response wind tunnel test, a dedicated device to produce the typical sinusoidal or *1-cos* gust profile as requested by the CS certification rules has been designed and manufactured. Since the test will be performed in the close chamber configuration, the capability of reaching the right gust velocity and a sufficient homogeneous gust field around the model has to be evaluated in the preliminary design phase, due to the wall effect and the dissipation of the gust along the chamber. The main design parameters playing a major role in the design of the gust generator are the number of gust vanes, its chord length, and the maximum rotation angle. Indeed, different and opposite requirements have to be combined. While the increase of the chord of the gust vane could potentially increase the maximum gust generated, the increased inertia of the vanes could limit the maximum frequency reachable. More, the increased number of the vanes could increase the maximum gust obtainable but at the same time generates disturbances in the normal flow even if when the vanes are not actuated. The final configuration obtained after an optimization process is based on the use of 6 vanes of $0.4m$ chord. Any couple of vanes is connected together and actuated by a single linear electromagnetic actuator, similar to one adopted for the WAS system. A dedicated control loop allows creating a *1-cos* gust profile. The 6 vanes have been manufactured by POLIMI using a single steel square tube as the main spar, the aerodynamic shape made by styrofoam and covered by glass fiber so to minimize the inertia and maximize the available excitation bandwidth [21].

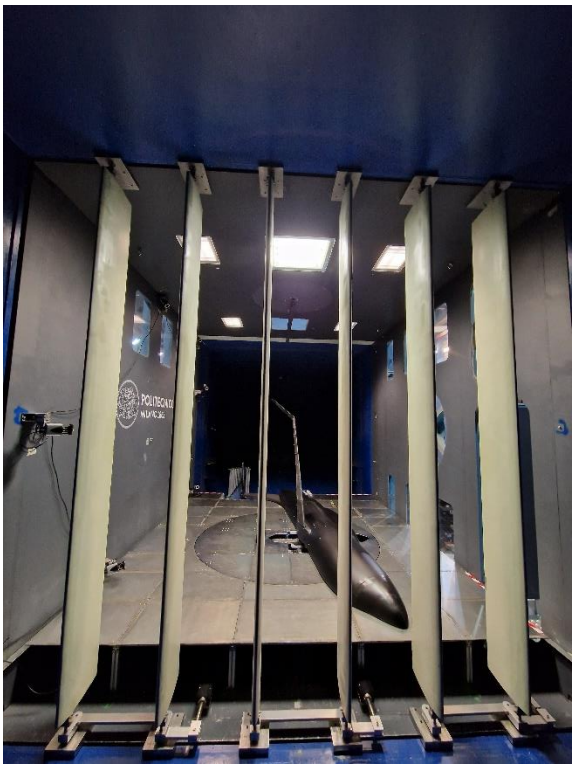

Figure 12: the gust generator

7 WIND TUNNEL TEST RESULTS

A variety of tests are performed, not just limited to gust response, but aiming at different goals, as summarized in the following:

- Check the difference in trim condition when the hinge is locked and unlocked.
- Compare root bending moment under gust excitation with the hinge locked and unlocked. This is done for different gust frequencies keeping the speed and the modulus of the amplitude of the gust constant.
- Investigate the different gust responses by introducing a known delay between the unlocking command of the hinge and the starting trigger of the gust. The speed is kept constant, while two different gust frequencies are tested.

7.1 Static trims

For the trim analysis in this wind tunnel configuration, we keep the model at the center of the sled. The electromagnetic actuator is controlled in position and the lift generated by the model is

measured by the load cell between the actuator and the model. The elevator deflection is modified until the value read by the load cell (the lift) is equal to (half) the scaled weight of the reference aircraft. At that point the output of every installed instrument is acquired for a fixed time period. This is also the starting point for every gust response test. The goal of this test is to evaluate the difference in angle of attack and elevator deflection between the locked and unlocked conditions.

This test is repeated for different speeds between 15 m/s and 25 m/s, where 15 m/s is just above the stalling speed for this wind tunnel model and 25 m/s is the scaled Vd of the reference aircraft. Since the architecture of the reference aircraft is different from the tested model, we are just interested in finding the main effects of unlocking the hinge and not in the actual values.

The difference in angle of attack and elevator deflection between the two conditions is reported in the following graph.

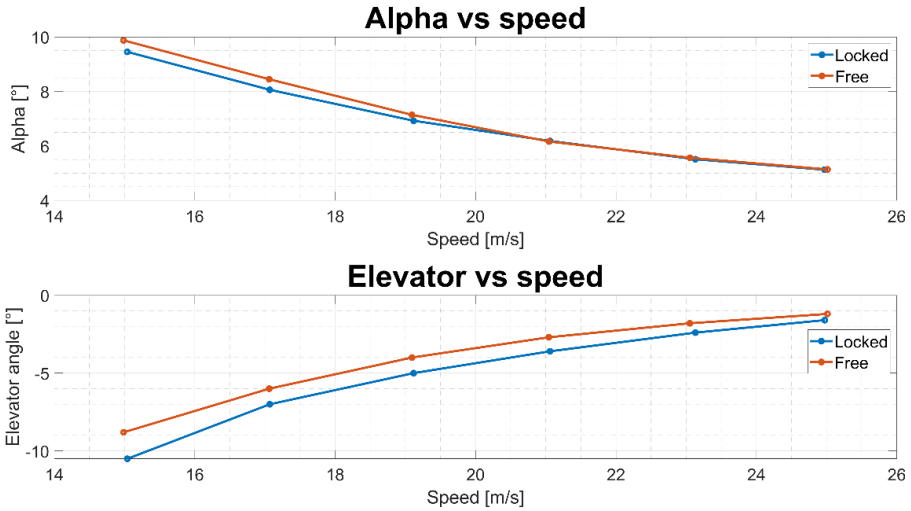

Figure 13: Angle of attack and elevator deflection over speed. Comparison between the locked and free wing tip conditions

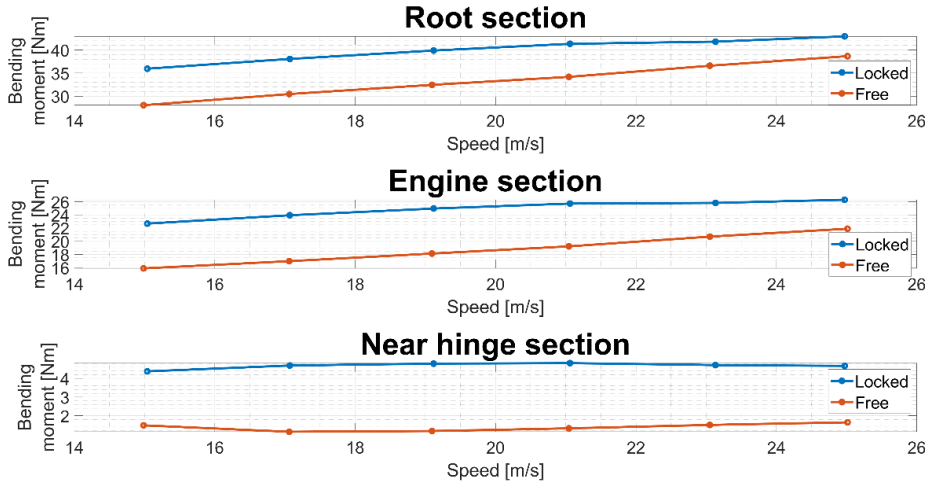

Figure 14: bending moment at three positions spanwise. Comparison between the locked and free wing tip conditions

7.2 Gusts with fixed/free wingtip

For the gust analysis, we start from the trimmed condition described earlier. Just before triggering the gust, the electromagnetic actuator control is switched from imposing a position to imposing the trim force. At this point, the model is free to fly when the gust arrives. In this part, we compare the internal actions due to the gust in two conditions: with the hinge locked and unlocked. There is no transient associated to the unlocking of the hinge, as the wing tip is free to float from the beginning. Here the test configuration doesn't allow to perfectly recreate the real behavior of the folding wing tip. The dummy weight applied by the electromagnetic actuator acts just on the rigid body motion of the model, but clearly not on the rigid rotation of the wing tip. For this reason, while trimming the aircraft with the hinge unlocked, the wing tip lays against the upper stopper due to the lift not being counteracted by the weight. In addition, the real weight pushes the wingtip against the stopper forming an inverted pendulum (and the acceleration of gravity is not scaled). As a result, when the gust hits the wingtip, a moment is transferred to the rest of the structure, contrary to the folding wing tip concept. As can be seen in the following graphs, an alleviation is still present due to the different starting point of the bending moment, but the peak itself is not alleviated but, rather, offset downward. All gusts are performed at 20 m/s, that is around the scaled Vc of the reference aircraft.

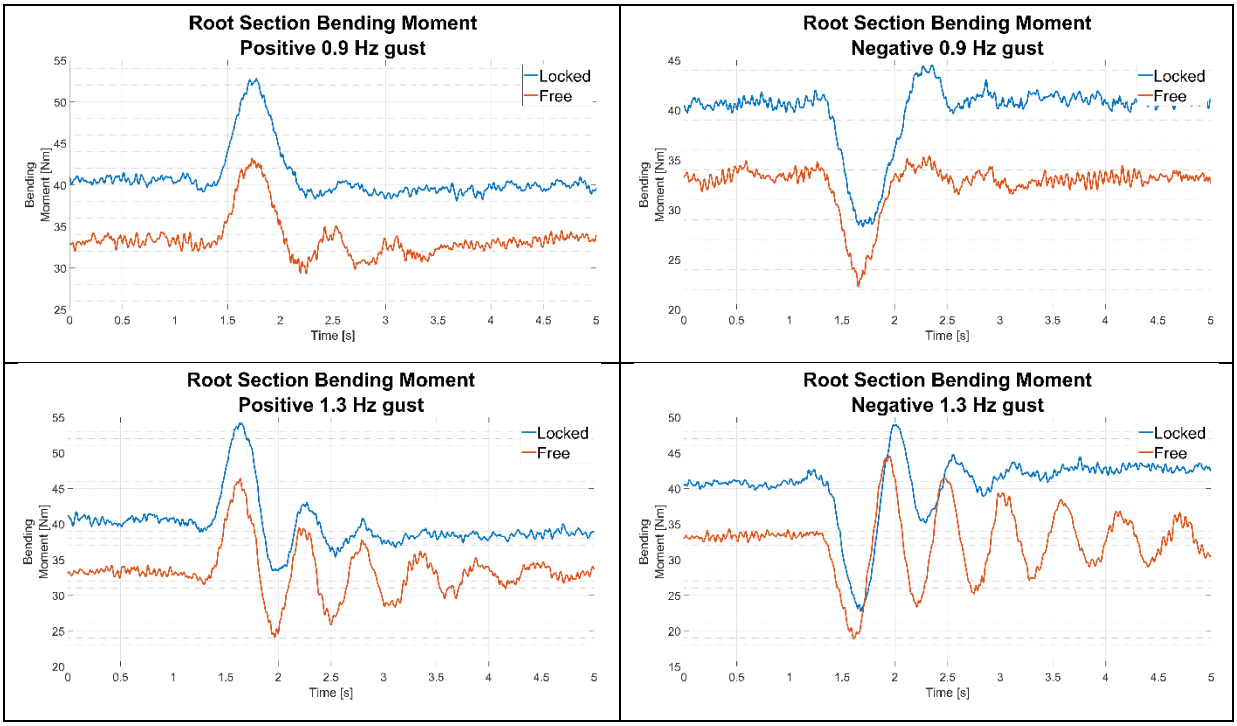

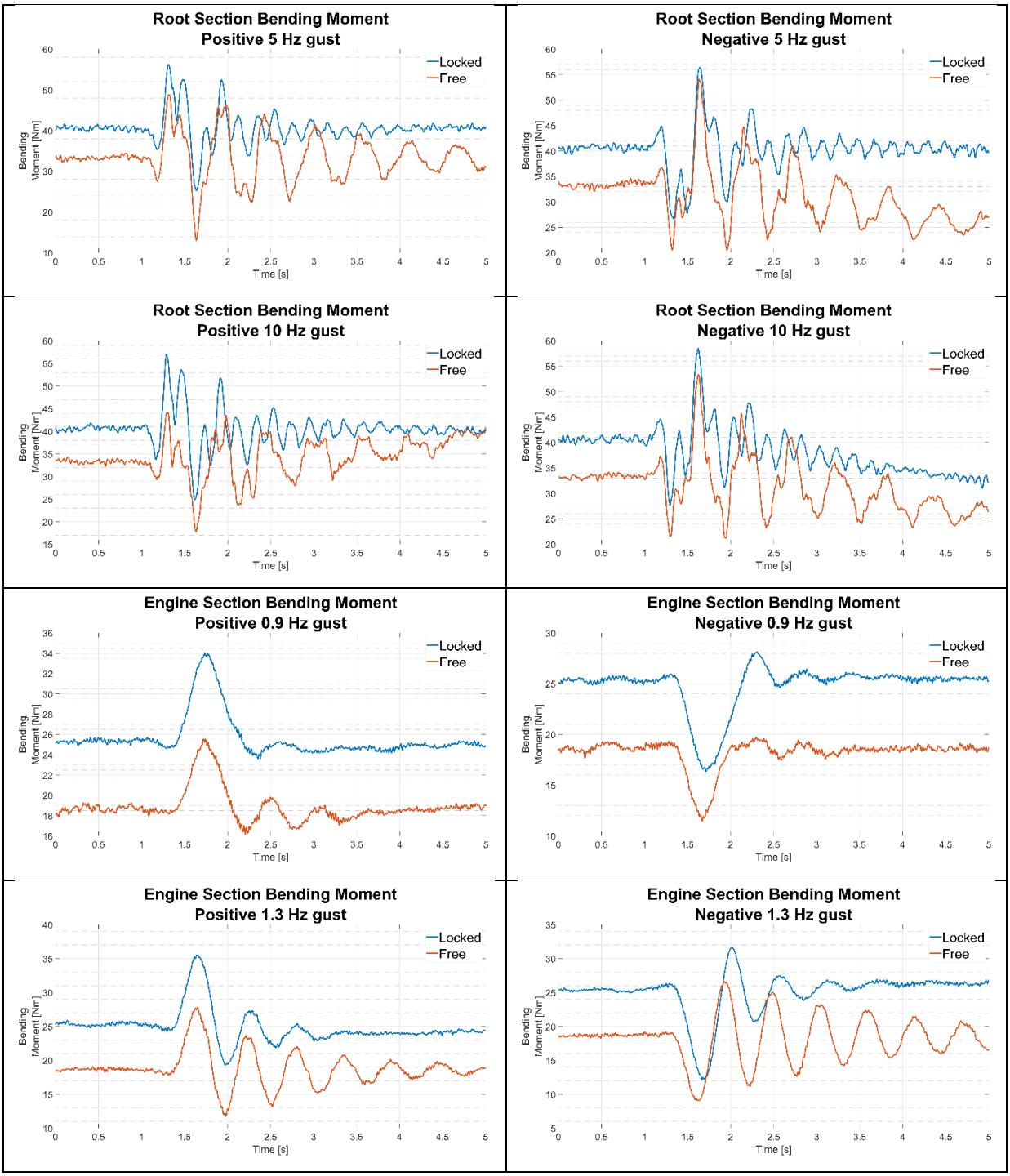
Root Section Bending Moment
Positive 5 Hz gust
Root Section Bending Moment
Negative 5 Hz gust
Root Section Bending Moment
Positive 10 Hz gust
Root Section Bending Moment
Negative 10 Hz gust
Engine Section Bending Moment
Positive 0.9 Hz gust
Engine Section Bending Moment
Negative 0.9 Hz gust
Engine Section Bending Moment
Positive 1.3 Hz gust
Engine Section Bending Moment
Negative 1.3 Hz gust
Locked
Free
Bending Moment [Nm]
Time [s]

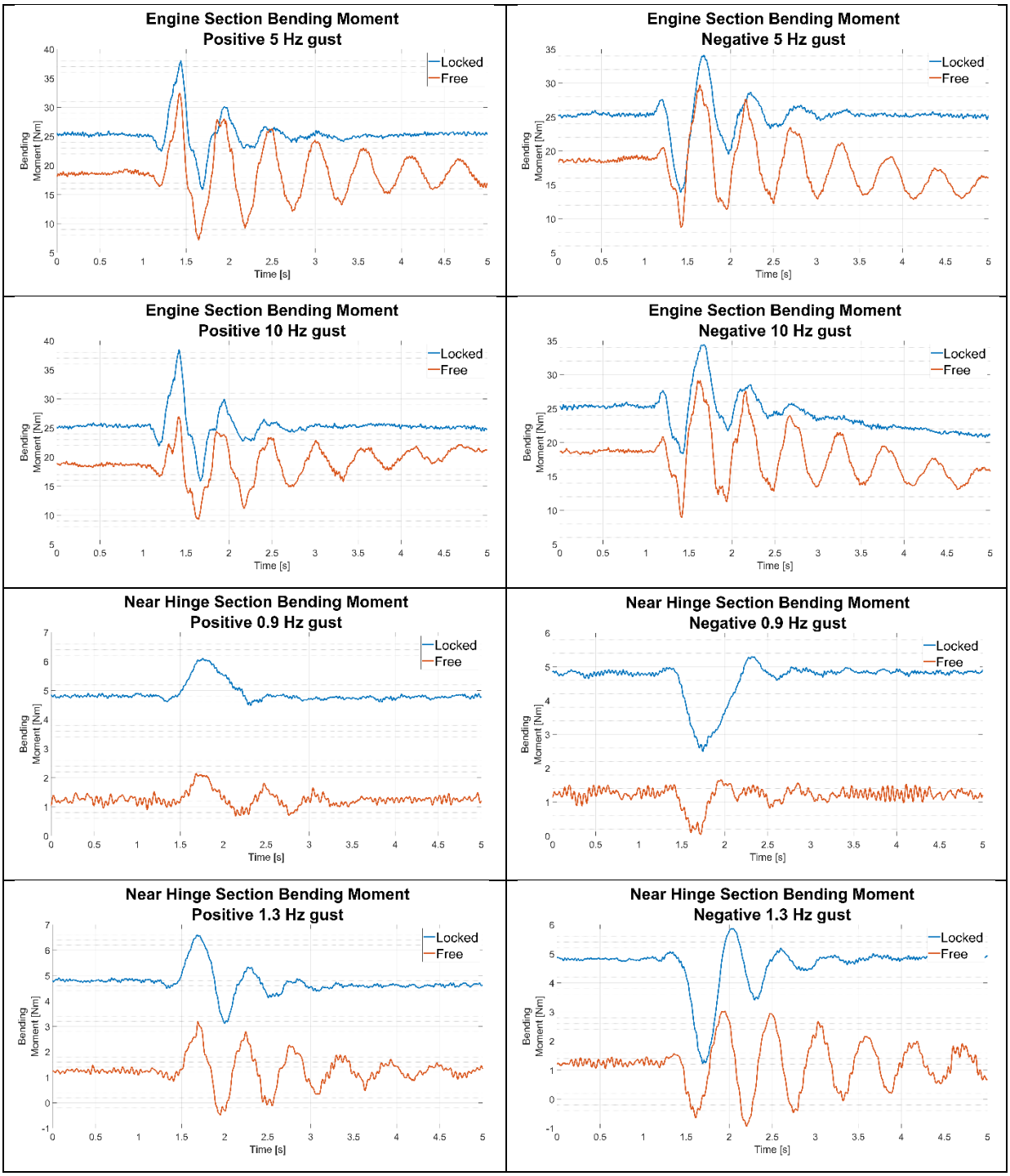
Engine Section Bending Moment
Positive 5 Hz gust
Engine Section Bending Moment
Negative 5 Hz gust
Engine Section Bending Moment
Positive 10 Hz gust
Engine Section Bending Moment
Negative 10 Hz gust
Near Hinge Section Bending Moment
Positive 0.9 Hz gust
Near Hinge Section Bending Moment
Negative 0.9 Hz gust
Near Hinge Section Bending Moment
Positive 1.3 Hz gust
Near Hinge Section Bending Moment
Negative 1.3 Hz gust
Locked
Free
Bending Moment [Nm]
Time [s]

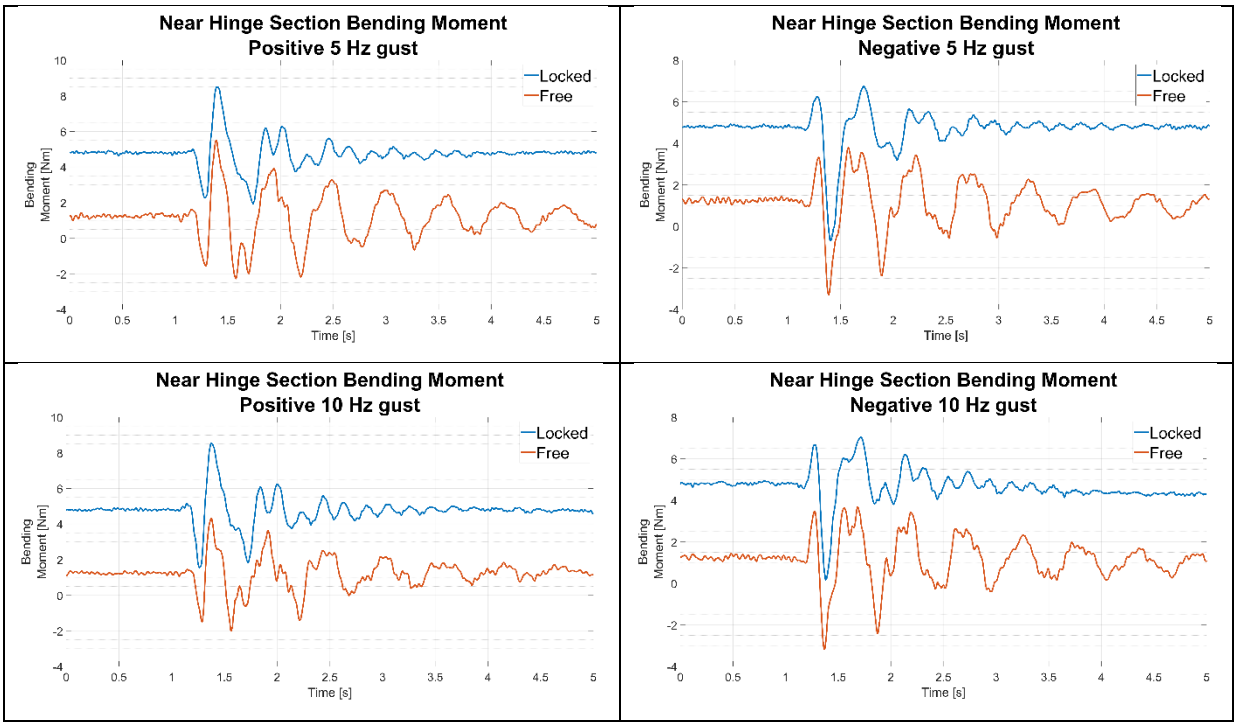

Figure 15: bending moment time history at three positions. Comparison between the locked and free wing tip conditions

7.3 Gusts with the dynamics of the unlocking

For this third analysis we introduce the dynamics of the unlocking of the hinge. With the same fixed speed used in the previous test, and just two different gust frequencies, we investigate the interaction between the dynamics of the wing tip due to the gust and the one due to the unlocking of the hinge. The same limitations previously discussed still apply, but the influence here should be smaller, because when the gust hits the wing tip, it should not be already pushing against the stopper. The delay reported in the graphs are the period between the trigger of the gust and the unlocking of the hinge. A positive delay means the gust is triggered before the hinge is unlocked. This does not necessarily mean that the gust hits the wing tip when the hinge is still locked, between the trigger of the gust and the gust actually hitting the wing tip there is the time it takes the gust to travel from the gust generator to the wing tip. All graphs are synchronized on the gust trigger, so the gust always starts at the same time, it's the unlocking of the hinge that changes.

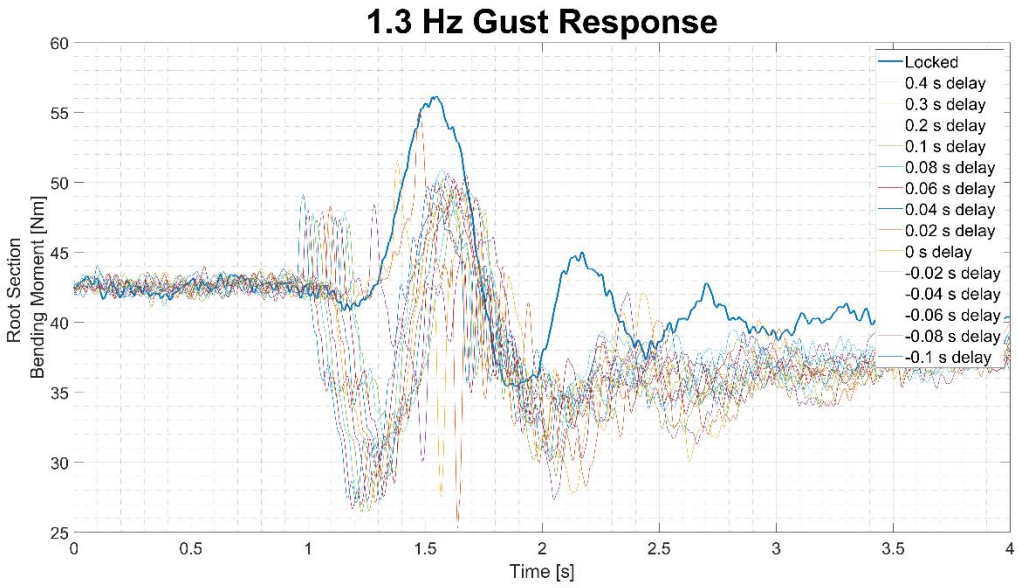

Figure 16: root bending moment time history. Comparison between the locked wing tip conditions and different time intervals between the gust and the unlocking of the wing tip

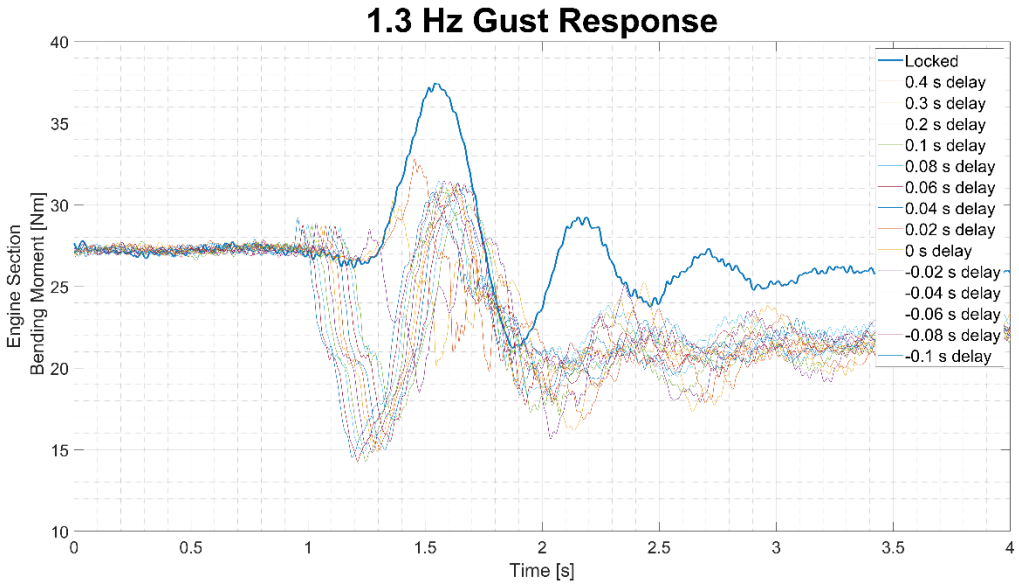

Figure 17: engine section bending moment time history. Comparison between the locked wing tip conditions and different time intervals between the gust and the unlocking of the wing tip

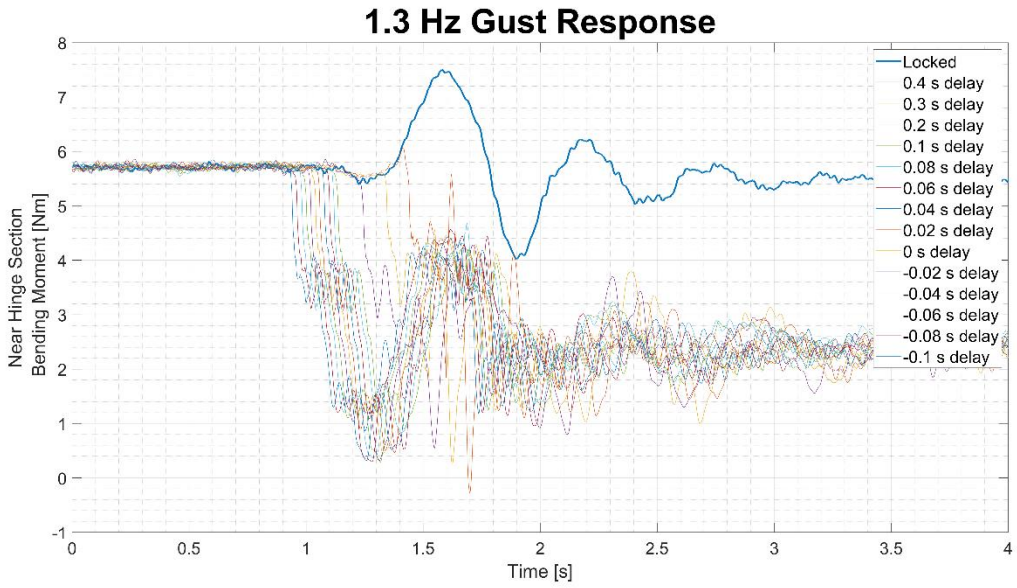

Figure 18: near hinge section bending moment time history. Comparison between the locked wing tip conditions and different time intervals between the gust and the unlocking of the wing tip

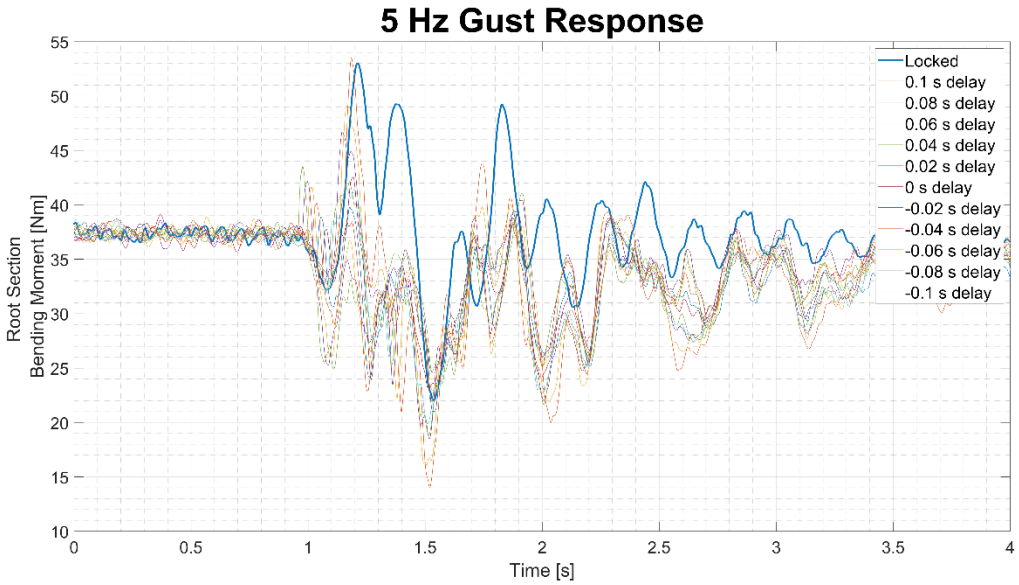

Figure 19: root bending moment time history. Comparison between the locked wing tip conditions and different time intervals between the gust and the unlocking of the wing tip

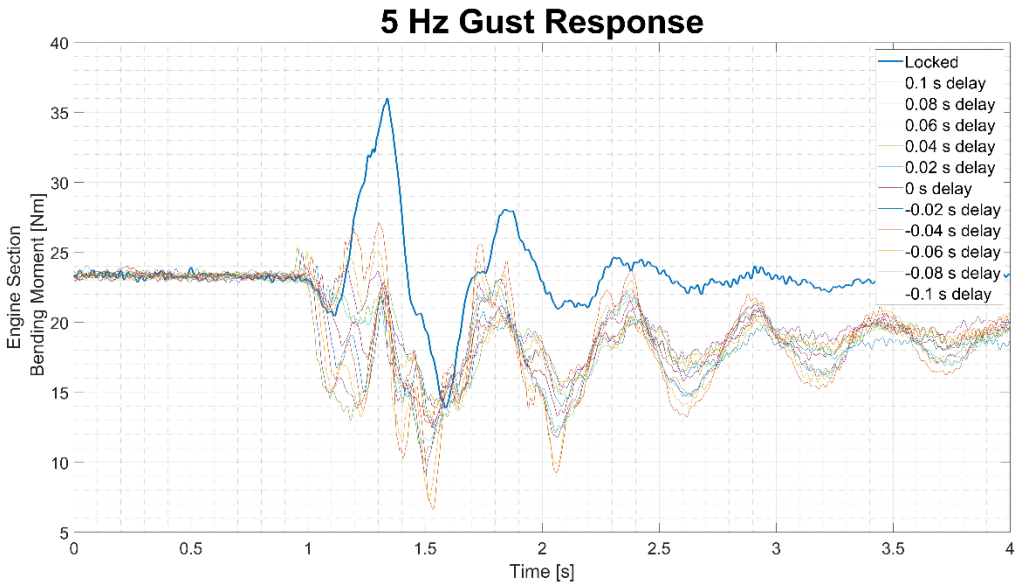

Figure 20: engine section bending moment time history. Comparison between the locked wing tip conditions and different time intervals between the gust and the unlocking of the wing tip

Figure 21: near hinge section bending moment time history. Comparison between the locked wing tip conditions and different time intervals between the gust and the unlocking of the wing tip

8 CONCLUDING REMARKS AND OUTLOOK

From the static aeroelasticity point of view, the main effect of the folding wing tip is on the aerodynamic moment, probably due to the large sweep angle of the wing. In the free-to-float wing tip condition the centre of pressure of the wing is pushed forward and a lower angle of elevator is required to trim the aircraft. Consequently, when the hinge is unlocked starting from a trimmed

condition, the angle of attack increases and the aircraft gains altitude. This effect can be compensated adjusting the elevator angle while the wingtip is unlocked.

A free-to-float folding wing tip is able to reduce the first peak of the root bending moment even in an unrealistic condition where it is always pushed against the stopper.

Table 3: max bending moment reduction in the always-free wing tip condition

Frequency [Hz]	Direction	Max Bending Moment Reduction
0.9	Positive	18%
0.9	Negative	21%
1.3	Positive	14%
1.3	Negative	9%
5	Positive	14%
5	Negative	4%
10	Positive	23%
10	Negative	9%

When we add the dynamics of the unlocking of the wing tip, the moment of the release with respect to the trigger of the gust has an influence on the amount of alleviation that is possible to obtain.

Table 4: max bending moment reduction depending on the interval between the unlocking of the wing tip and the gust. 1.3 Hz gust

Frequency [Hz]	Direction	Delay [s]	Max Bending Moment Reduction
1.3	Positive	0.4	1.9%
1.3	Positive	0.3	8.1%
1.3	Positive	0.2	13.8%
1.3	Positive	0.1	14.1%
1.3	Positive	0.08	11.9%
1.3	Positive	0.06	10.0%
1.3	Positive	0.04	11.6%
1.3	Positive	0.02	11.7%
1.3	Positive	0	11.7%
1.3	Positive	-0.02	9.8%
1.3	Positive	-0.04	10.5%
1.3	Positive	-0.06	9.3%
1.3	Positive	-0.08	11.3%
1.3	Positive	-0.1	10.7%

Table 1: max bending moment reduction depending on the interval between the unlocking of the wing tip and the gust. 5 Hz gust

Frequency [Hz]	Direction	Delay [s]	Max Bending Moment Reduction
5	Positive	0.1	-0.9%
5	Positive	0.08	7.4%
5	Positive	0.06	11.9%
5	Positive	0.04	20.5%
5	Positive	0.02	21.1%
5	Positive	0	19.7%

5	Positive	-0.02	25.0%
5	Positive	-0.04	24.2%
5	Positive	-0.06	21.4%
5	Positive	-0.08	20.4%
5	Positive	-0.1	17.9%
5	Positive	0.1	-0.9%
5	Positive	0.08	7.4%
5	Positive	0.06	11.9%

At the end of this complex experimental campaign, it is possible to draw some partial conclusions. At first, the root bending moment reduction experimentally obtained during the large experimental campaign are in line with the numerical estimations. The experimental apparatus proved to be extremely effective and reliable. In particular, the possibility of re-engaging the locking mechanism in a few seconds, simply by varying the angle of attack of the model, exploiting the aerodynamics of the wing tip, proved fundamental in being able to carry out the tests continuously without having to turn off the wind tunnel. Despite the absence of any specific active control system, playing with the delay between the gust activation and the release mechanism showed the potential to directly controlling the maximum root bending load. A deep post testing investigation is necessary and will be conducted in the next months.

9 ACKNOWLEDGEMENTS

This project U-HARWARD has received funding from the Clean Sky 2 Joint Undertaking (JU) under grant agreement No 886552. The JU receives support from the European Union's Horizon 2020 research and innovation programme and the Clean Sky 2 JU members other than the Union.

10 REFERENCES

[1] "Work programme 2013 Cooperation Theme 7 Transport (including Aeronautics)," European Commission C (2012) 4536 of 9 July 2012.

[2] "European Aeronautics: A Vision for 2020.," Group of Personalities, ISBN 92-894-0559-7.

[3] "ACARE Strategic, Research and Innovation Agenda Vol 1," Realising Europe's Vision for Aviation, 2012.

[4] Aerospace_Technology_Institute, ATI Technology Strategy - Destination Zero, 2022.

[5] ATAG, Waypoint 2050. A Vision of Net Zero Aviation by Mid Century, 2021.

[6] A. Castrichini, V. H. Siddaramaiah, D. Calderon, J. Cooper, T. Wilson and Y. Lemmens, "Preliminary Investigation of Use of Flexible Folding Wing-Tips for Static and Dynamic Loads Alleviation," *Aeronautical Journal*, 2016.

[7] R. Cheung, D. Rezgui, J. E. Cooper and T. Wilson., "Testing of a Hinged Wingtip Device for GustLoads Alleviation," *Journal of Aircraft*, vol. 55, pp. 2050-2067, 2018.

[8] R. Cheung, D. Rezgui, J. Cooper and T. Wilson, "Testing of Folding Wingtip for Gust Load Alleviation of Flexible High-Aspect-Ratio Wing," *Journal of Aircraft*, 2020.

[9] F. Healy, R. Cheung, D. Rezgui, J. Cooper, T. Wilson and A. Castrichini, "On the Effect of Geometric Nonlinearity on the Dynamics of Flared Folding Wingtips," *Journal of Aircraft*, vol. 60, pp. 368-381, 2023.

[10] F. Healy, R. Cheung, D. Rezgui, J. Cooper, T. Wilson and A. Castrichini, "Experimental and Numerical Nonlinear Stability Analysis of Wings Incorporating Flared Folding Wingtips," *Journal of Aircraft*, pp. 1-15, 2023.

[11] F. Healy, R. Cheung, T. Neofet, M. Lowenberg, D. Rezgui, J. Cooper and A. C. a. T. Wilson, "FoldingWingtips for Improved Roll Performance," *Journal of Aircraft*, 2021.

[12] T. Wilson, "Update on AlbatrossONE Semi Aeroelastic Hinge Small Scale Flying Demonstrator Project," *International Forum on Aeroelasticity and Structural Dynamics*, 2022.

[13] A. Castrichini, T. Wilson and J. and Cooper, "On the Dynamic Release of the Semi Aeroelastic Wing-Tip Hinge Device," *6th RAeS Aircraft Structural Design Conference, Royal Aeronautical Society*, 2018.

[14] A. Castrichini, H. Siddaramaiah, D. V. Calderon, C. J., T. Wilson and Y. and Lemmens, "Nonlinear Folding Wing Tips for Gust Loads Alleviation," *Journal of Aircraft*, vol. 53, p. 1391– 1399, 2016.

[15] H. Gu, F. Healy, S. Jayatilake, D. Rezgui, M. Lowenberg, J. E. Cooper, T. Wilson and A. Castrichini, "Flight dynamics of aircraft incorporating the semi-aeroelastic hinge," *Aerospace Science and Technology*, 2024.

[16] X. Carrillo, C. Mertens, A. Sciacchitano, B. v. Oudheusden and R. D. B. a. J. Sodja, "Wing Stiffness and Hinge Release Threshold Effects on Folding Wingtip Gust Load Alleviation," *AIAA SCITECH 2022 Forum.*

[17] J. E. Cooper, H. Gu, S. Ricci, F. Toffol, S. Adden, M. Meheut, E. Benard and P. Barabinot, "CS2-THT U-HARWARD Project: Final Assessment and Project Outcomes Evaluation," in *AIAA Scitech Forum*, Orlando, FL, January 2024.

[18] F. Toffol, L. Marchetti, A. De Gaspari, J. V. Chardi Espi, L. Riccobene, F. Fonte, S. Ricci and P. Mantegazza, "Design and Experimental Validation of Gust Load Alleviation Systems based on Static Output Feedback," in *AIAA SciTech Forum*, San Diego, CA, January 2022.

[19] F. Toffol, L. Marchetti, S. Ricci, F. Fonte, E. Capello and S. Malisani, "Gust and Manouvre Loads Alleviation Technologies: Overview, Results and Lesson Learned in the Framework of the CS2 Airgreen2 Project," in *IFASD*, Madrid, Spain, June 2022.

[20] S. Ricci, A. De Gaspari, L. Riccobene and F. Fonte, "Design and wind tunnel test validation of gust load alleviation systems," in *58th AIAA/ASCE/AHS/ASC Structures, Structural Dynamics, and Material Conference*, Grapevine, TX, USA, January 2017.

[21] F. Fonte, L. Riccobene, S. Ricci, S. Adden and M. Martegani, "Design, Manufacturing and Validation of a Gust Generator for Wind Tunnel Test of a Large Scale Aeroelastic Model," in *30th Congress of the International Council of the Aeronautical Science*, Daejeon, September 2016.

COPYRIGHT STATEMENT